RSC Advances

PAPER

View Article Online
View Journal | View Issue

Cite this: *RSC Adv.*, 2023, **13**, 2561

A novel supramolecular Zn(II)-metallogel: an efficient microelectronic semiconducting device application†

Kripasindhu Karmakar, ‡[a] Arka Dey,‡[b] Subhendu Dhibar, *[a] Rajib Sahu,[c] Subham Bhattacharjee,[d] Priya Karmakar,[a] Priyajit Chatterjee,[e] Aniruddha Mondal [b] and Bidyut Saha *[a]

Received 20th November 2022
Accepted 10th January 2023

DOI: 10.1039/d2ra07374a

rsc.li/rsc-advances

A unique strategy for the synthesis of a supramolecular metallogel employing zinc ions and adipic acid in DMF medium has been established at room temperature. Rheological analysis was used to investigate the mechanical characteristics of the supramolecular Zn(II)-metallogel. Field emission scanning electron microscopy and transmission electron microscopy were used to analyse the hexagonal shape morphological features of the Zn(II)-metallogel. Interestingly, the electrical conductivity is observed in the electronic device with Zn(II)-metallogel based metal–semiconductor (MS) junctions. All aspects of the metallogel's electrical properties were investigated. The electrical conductivity of the metallogel-based thin film device was 7.38 × 10^{-5} S m^{-1}. The synthesised Zn(II)-metallogel based device was investigated for its semi-conductive properties, such as its Schottky barrier diode nature.

1. Introduction

The study of supramolecular gels is one of the most exciting and promising areas of research in the field of supramolecular chemistry and materials science. Gels are solids with a high degree of viscoelasticity; they are made up of an elastic as well as cross-linked network and a solvent. The liquid is entrapped and adheres to the vast surface area of the three-dimensional solid matrix, giving the gel a solid-like appearance.[1,2] Several non-covalent interactions such as hydrophobic contacts, van der Waals forces, cation···π, anion···π, π···π, hydrogen bonding, dipole–dipole, ion–ion, and dipole–dipole interactions *etc.* have been crucial to the generation of supramolecular networks.[3,4] The direct use of supramolecular phenomena has facilitated the development of 3D soft gel scaffolds.[5] To create a stable gel architecture with different gelators, a wide variety of polar type solvents, like water,[6] methanol,[7] ethanol,[8] dimethyl sulfoxide,[9] acetonitrile,[10] *N*,*N*-dimethyl formamide,[11] and nonpolar solvents, such as tetrahydrofuran,[12] toluene,[13] acetone,[14] carbon tetrachloride,[15] 1,2 dichlorobenzene,[16] dichloromethane,[17] deuterated dichloromethane[18] solvents are very effective.

As supramolecular type soft scaffolds, low-molecular-weight gelators (LMWGs) with a molecular weight of ≤3000 have been introduced into synthetic gel systems along with the polymeric gelator-based gel. Despite various low molecular weight gelators such as alkenes,[19] saccharides,[20] sugars,[21] urea derivatives,[22] modified amino acids,[23] peptides,[24] bile acids,[25] carbohydrate,[26] cholesterol,[27] and amides[28] are general in the chemistry of gelation, achieving the necessary and effective synthesis utilising LMWGs remains still difficult. Along with the demonstration of the supramolecular gelation process, the current direction in gel research[29] is the introduction of metal ions along with the LMWGs for the formation of multifunctional supramolecular metallogels. The combination of diverse metal ions and organic components of low molecular weight combine to generate metallogels with distinct self-aggregation mechanisms and non-covalent characteristics, which lead to the development of more compelling and remarkable properties in the domain of science and technology. Supramolecular metallogels have significant applications in a wide range fields of materials science, including the food industry, cosmetics, electron emission, photophysics, logic gates, drug delivery, cell culturing, biomineralization, medical diagnostics, tissue engineering, lithography, optical activity, energy storage, charge transportation, catalysis, conductivity, actuators, magnetic materials, redox responsiveness, chemosensors, electrochemical and optoelectronic devices, nanoscience and nanoelectronics *etc.*[30–49]

[a]*Colloid Chemistry Laboratory, Department of Chemistry, The University of Burdwan, Golapbag, Burdwan-713104, West Bengal, India. E-mail: sdhibar@scholar.buruniv.ac.in; bsaha@chem.buruniv.ac.in; Tel: +91 7001575909; +91 9476341691*

[b]*Department of Physics, National Institute of Technology Durgapur, Durgapur-713209, West Bengal, India*

[c]*Max-Plank-Institut für Eisenforschung GmbH, Max-Plank-Str. 1, 40237 Düsseldorf, Germany*

[d]*Department of Chemistry, Kazi Nazrul University, Asansol-713303, West Bengal, India*

[e]*University Science Instrumentation Centre, The University of Burdwan, Golapbag, Burdwan-713104, West Bengal, India*

† Electronic supplementary information (ESI) available: TEM image of Zn-AA metallogel. See DOI: https://doi.org/10.1039/d2ra07374a

‡ K. K. and A. D. should be treated as joint first authors.

Recent emphasis has been focused on supramolecular metallogel systems based on transition metals as smart functional materials owing to their affordability and availability. Multiple transition metal ion-based metallogels involving Cu, Ni, Fe, Mn, Co, *etc.* are documented in the scientific literature.[50–55] Zn(II) is one of the most important transition metal ions for numerous successful applications in catalysis,[56] cell imaging,[57] and medicinal chemistry[58] *etc.*

Functional LMWG based supramolecular gels may be synthesised using the concept that adipic acid has metallogel forming capacity in DMF solvent media. We have used a method called adipic acid-mediated gel formation in this endeavour. Here, we investigate the susceptibility of adipic acid to metallogelation using Zn(II) as a source in *N*,*N*-dimethylformamide under ambient conditions. A new supramolecular Zn(II)-metallogel (Zn-AA) is facilitated by the presence of adipic acid. Adipic acid may look promising as a LMWG towards a wide variety of metal ions since the adipate ion may serve as a chelating ligand as well as a bridging ligand.

Researchers in the field of materials science are always exploring for opportunities to create innovative forms of energy storage and conversion technology. The discovery of the functional material mediated by metallogels is a major advance in this field. The mechanical flexibility and soft chemical nature of metallogels opens up a wide range of possible applications.[59]

Herein, we have tested the feasibility of using Zn-AA metallogel in devices, since in the semiconducting area, this material provides a considerable optical band gap. Implementing these materials in real-world electrical devices is a technical challenge. We have successfully used Zn(II) metallogel material in the metal–semiconductor junction thin film devices to investigate the capability for transporting charge and adaptability of electronic device. Schottky behaviour with potential photosensing activity using readily accessible, low-cost transition metal ions has been shown in a synthetic material-based metal semiconductor (MS) junction device. Our constructed devices show a non-linear rectifying nature in their current–voltage characteristics graph, much like a Schottky barrier diode with a significant rectification ratio. As a result, we have evaluated the functionality of the Schottky diode we built using Zn-AA metallogel. Research into the material's photophysical and electronic charge transport properties demonstrates its potential to pique the interest of future scientists developing metallogel-based active electronic devices.

2. Experimental

2.1. Materials

Adipic acid and zinc(II) acetate dihydrate were bought from Sigma-Aldrich Company and they were utilised exactly as supplied. The whole experiment was executed using *N*,*N*-dimethyl formamide (DMF) solvent.

2.2. Characterizations

A SHIMADZU UV-3101PC spectrophotometer was utilized for the UV-vis absorption spectrum data.

Rheological studies: for rheology experiment of the gels, an Anton Paar 100 rheometer with a cone and plate geometry (CP 25-2) having an adjustable Peltier temperature controlling system was used. All the measurements were done fixing the gap distance between the cone and the plate at 0.05 mm. The gels were scooped on the plate of the rheometer. An oscillatory strain amplitude sweep experiment was performed at a constant oscillation frequency of 1 Hz for the applied strain range 0.001–10% at 20 °C. The software US-200 converted the torque measurements into either G' (the storage modulus) and G'' (the loss modulus) and represent G' and G'' with either strain or shear stress. Oscillatory frequency sweep experiments were performed in the linear viscoelastic region (strain 0.01%) to ensure that calculated parameters correspond to an intact network structures.

A Carl Zeiss SUPRA 55VP FESEM instrument was utilized to perform the field emission scanning electron microscope (FESEM).

Transmission electron microscopy (TEM) was performed using a ThermoFisher image corrected Titan Themis at an operating voltage of 300 kV. A Bruker SuperX detector was used for the energy-dispersive X-ray spectroscopy (EDX) study in scanning TEM mode (STEM). TEM sample was prepared by sonication in ethanol.

For the IR investigation, a Shimadzu FTIR-8400S FTIR spectrometer was used.

The Phillips PANalytical X'PERT PRO equipment was utilized to acquire the Powder X-Ray Diffraction (PXRD) data of the Zn-AA metallogel at room temperature.

A digital melting point measuring apparatus Aplab (model: MPA-01) was used to determine the T_{gel} of the Zn-AA metallogel.

Our synthesised metallogel material-based thin film device's current–voltage (*I*–*V*) characteristics were performed using a Keithley 2401 source meter.

2.3. Synthesis of Zn(II)-metallogel (Zn-AA)

At room temperature, 0.219 g of Zinc(II) acetate dihydrate (1 mmol) in ~1 mL of DMF and 0.292 g of adipic acid (2 mmol) in ~1 mL of DMF were combined. Therefore, a white, stable gel of Zn(II) (*i.e.* Zn-AA) was formed by sonicating the vial for 5 minutes at ambient temperature and air pressure (Fig. 1).

3. Results and discussion

3.1. Evaluation of the gel-melting temperature (T_{gel}) and the minimum critical gelation concentration (MGC)

The assessment of the Zn-AA metallogel's minimum critical gelation concentration (MGC) is shown in Fig. 2. To assess the

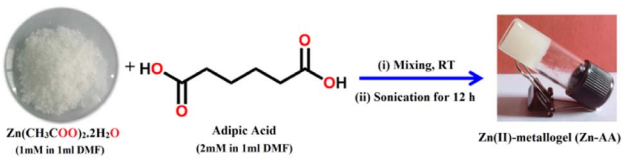

Fig. 1 Representation of the gelation process of Zn(II)-metallogel.

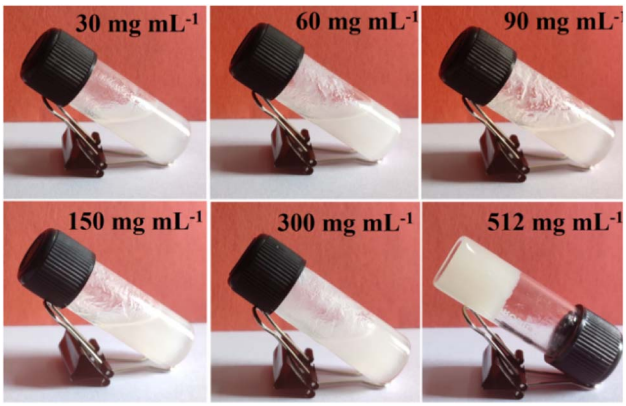

Fig. 2 Photographic illustration of the Zn-AA metallogel gelating at the minimal critical concentration (MGC). MGC is 512 mg mL^{-1} when compared to the 1 : 2 (w/w) weight ratio of $Zn(CH_3COO)_2 \cdot 2H_2O$ and adipic acid.

MGC of the Zn-AA metallogel, the concentrations of $Zn(CH_3COO)_2 \cdot 2H_2O$ and adipic acid were altered within a range of concentration (*i.e.* 30 mg mL^{-1} to 512 mg mL^{-1}). Here, $[Zn(CH_3COO)_2 \cdot 2H_2O]$: [adipic acid] = 1 : 2, (w/w), was retained as the constituent ratio for the Zn-AA metallogel. 512 mg mL^{-1} of Zn(II)-acetate salt and adipic acid in DMF solvent produced the stable and white Zn-AA metallogel (Fig. 2).

The gel melting temperature (T_{gel}) of Zn-AA metallogel was recorded as ~120 °C ± 2 °C by digital melting point measuring apparatus.

3.2. Rheological analysis

Rheological measurements were used to determine the semi-solid and viscoelastic nature of Zn-AA metallogel (Fig. 3). The storage modulus and the loss modulus of the metallogel are denoted by G' and G'' respectively. They are represented by the equations

$$G' = (\sigma_0/\gamma_0)\cos(\delta)$$

$$G'' = (\sigma_0/\gamma_0)\sin(\delta)$$

For any gel material the condition $G'(\omega) > G''(\omega)$ is valid [where, $G'(\omega) \approx \omega^{\circ}$ and ω represents the angular frequency].

Keeping the $Zn(OAc)_2 \cdot 2H_2O$ concentration constant (*i.e.* [Zn(II)] = 512 mg mL^{-1}), rheological studies demonstrated that the value of storage modulus of Zn-AA metallogel is much higher than the value of loss modulus, *i.e.* ($G' > G''$) (Fig. 3). The Zn-AA metallogel is found to have a significantly high storage modulus ($G' > 10^6$ Pa) that is much greater than its loss modulus (G''), which is reconcilable with the material maintaining its gel structural characteristic, semisolid-like behaviour, and large tolerance limit (Fig. 3). Fig. 4 displays the results of a strain-sweep measurement of Zn-AA metallogel at a fixed 6.283 rad s^{-1} frequency.

3.3 Microstructural study

The field emission scanning electron microscopic (FESEM) pattern of the Zn-AA metallogel showed the agglomerated hexagonal like hierarchical network of the metallogel (Fig. 5a and b).

The structural concreteness in microstructural network of Zn-AA metallogel might be due to the predominant supramolecular interactions. Bright field TEM image reveals a mixed hexagonal and pentagonal shaped structural morphology of Zn-AA metallogel in Fig. 5c. The average range in length and width is measured around 200–400 nm and 120–320 nm for hexagonal and 160–220 nm and 200 nm in pentagonal structure, respectively. Along with hexagonal morphology, a rod shape feature is found in minor quantity. Please see Fig. S1 in ESI† for the rod shape morphological pattern along with its chemical composition mapping by STEM EDX. Elemental composition mapping by STEM EDX in Fig. 5d–h confirms presence of Zn, N, C and O elements of $Zn(OAc)_2 \cdot 2H_2O$, adipic acid and DMF molecules, which are used in preparation of Zn-AA metallogel (Fig. 5d).

3.4 FT-IR and PXRD analysis of Zn-AA metallogel

The Fourier transform infrared (FT-IR) spectra of Zn-AA metallogel in its xerogel form discloses the major absorption peaks are located at 2950, 2875, 1690, 1530, 1446, 1401, 1341, 1273, 1221, 1045, 906, 740, 690 and 520 cm^{-1} *etc.* (Fig. 6). The high

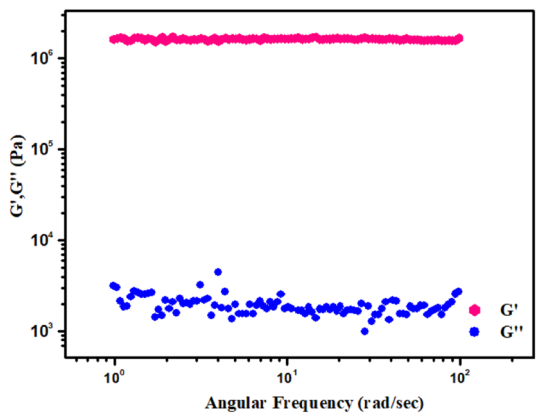

Fig. 3 Variation of G' and G'' (Pa) of Zn-AA metallogel.

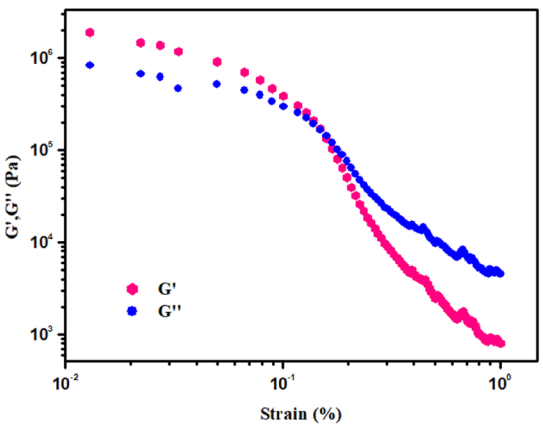

Fig. 4 Strain-sweep measurements of Zn-AA metallogel.

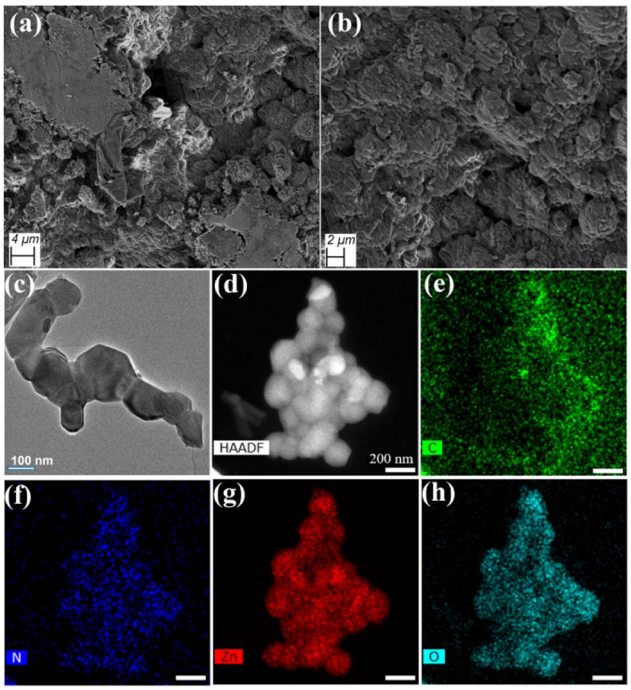

Fig. 5 Zn-AA metallogel: (a and b) the FESEM microstructural pattern of Zn-AA metallogel, (c) bright field TEM image of Zn-AA metallogel. (e–h) Elemental composition of C, N, Zn and O are mapped by STEM EDX. The corresponding region is shown in STEM image (d).

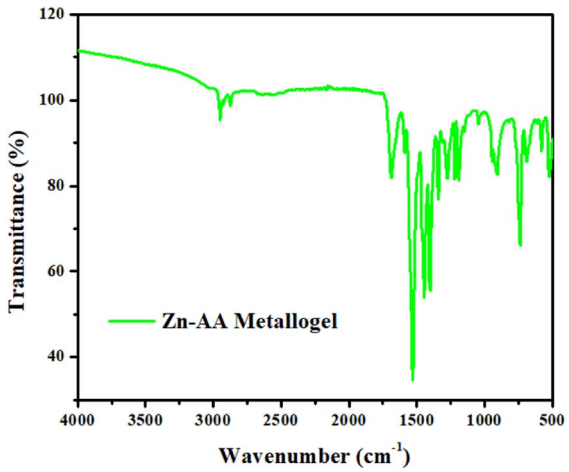

Fig. 6 FT-IR spectra of the xerogel form of Zn-AA metallogel.

intensity peak at 1690 cm^{-1} is obtained because of the asymmetric stretching vibration of carbonyl group (C=O) of acetate. The O–H stretching and the C–H stretching at 2950 cm^{-1} and 2875 cm^{-1}, are both excellent indicators of the existence of adipic acid. Fig. 6 displays the FT-IR spectra of Zn-AA metallogel. The (O–C=O) vibration mode and C=O symmetric stretching are attributed to the peak at 1530 cm^{-1}. The C–H bond vibration and C–O stretching modes are responsible for the numerous absorption peaks seen at 1446 cm^{-1}, 1401 cm^{-1}, 1341 cm^{-1}, 1273 cm^{-1} and 1221 cm^{-1}. The C–C stretching modes of vibration are responsible for a sequence of FTIR bands at 906 cm^{-1} and 1045 cm^{-1}. The band at 740 cm^{-1}, confirms the OH out of plane bending. The absorption frequency at 690 cm^{-1} is associated with the COO bending mode. The spectrum depicts a peak at 520 cm^{-1} that is obtained because of the presence of Zn–O bond and it confirms the formation of the metallogel. Fourier transform infrared (FT-IR) spectral data displays the supramolecular interactions in Zn-AA metallogel among the metallogel forming chemical components.

The powder X-ray diffraction is utilized to find out the structural nature of Zn-AA metallogel (Fig. 7). The crystalline character of the Zn(II)-metallogel is indicated by the PXRD pattern of sharp and narrow peaks. As shown in Fig. 7, the sharp XRD peaks appearing at $2\theta = 25.2$, 27.0, 29.1°, 39.0°, 49.0°, and 60.2° confirms the crystalline nature of Zn-AA metallogel gel. Further the XRD patter is compared with the standard data (JCPDS card # 372718) of zinc dicarboxylate, and is indexed accordingly. All these results confirm the crystalline nature of Zn-AA metallogel gel due to presence of zinc dicarboxylate.

3.5 Device fabrication

To make metallogel-based thin film devices (MBDs), glass substrates with indium-doped tin oxide (ITO) coatings were subjected to standard wet cleaning techniques utilising an ultrasonic cleaner in a soap solution, deionized water followed by isopropanol and acetone for 15 minutes each, before finally being annealed in 70 °C in the presence of N_2 for 15 minutes. For performing the electrical properties measurement multiple metal–semiconductor (MS) junction devices having the configuration like sandwich *i.e.* ITO/Zn-AA metallogel/Au were developed. The thin film of as-synthesized compound was pasted on the pre cleaned ITO-coated glass substrate by doctor blading method. Here the gold (Au) was used as the metal electrode, which was deposited on a precleaned plain glass slide by using a thermal evaporator unit under the base pressure of 10^{-6} Torr.

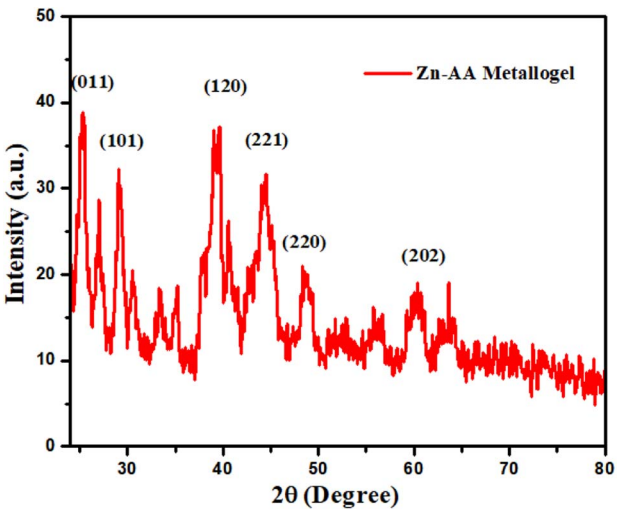

Fig. 7 Powder X-ray diffraction (PXRD) pattern of Zn-AA metallogel in xerogel form.

Electrical parameters were analysed by measuring the device's current–voltage (*I–V*) characteristics using a Keithley Sourcemeter (model no. 2401) and the two-probe method. All of the devices were built and tested under ambient circumstances at room temperature (28 °C).

3.6 Optical characterization

The optical band gap (E_g) of our Zn-AA metallogel was determined by using Tauc's equation (eqn (1)).[60]

$$\alpha h\nu = A(h\nu - E_g)^n \quad (1)$$

where ν, h, E_g and α stand for frequency of light, Planck's constant, optical band gap and absorption coefficient respectively. The exponent 'n' is the constant which depends on the process of electron transition. For ideal case the value of 'A' is considered as 1. The direct optical band gap has been computed using the aforementioned equation with an appropriate exponent value $n = \frac{1}{2}$.[60] The values of optical direct band gap (E_g) have been computed as 3.52 eV for our synthesized Zn-AA metallogel by extrapolating the straight line portion of $(\alpha h\nu)^2$ *vs.* $h\nu$ graph (Fig. A) to $\alpha = 0$ absorption.

The analysis of the optical properties of Zn-AA metallogel was executed using UV-Vis spectroscopy. From the obtained UV-Vis absorption spectra (inset of Fig. 8), the band gap (optical) (E_g) of the metallogel was determined. From Tauc's equation (eqn (1)),[60] the E_g was computed as 3.52 eV (Fig. 8). The obtained spectrum determined that the band gap of compound (1) is a direct type.

3.7 Electrical characterization

The just computed band gap value suggested our synthesized metallogel from the semiconductor family. Therefore, to study its electrical properties, Metal (Al)–Semiconductor (metallogel) (MS) junction thin-film devices were fabricated followed by the procedure described in device fabrication part. The current–voltage (*I–V*) graph of metallogel-based devices (MBDs) was performed with bias voltage applied in the span of ±2 V at room temperature (28 °C).

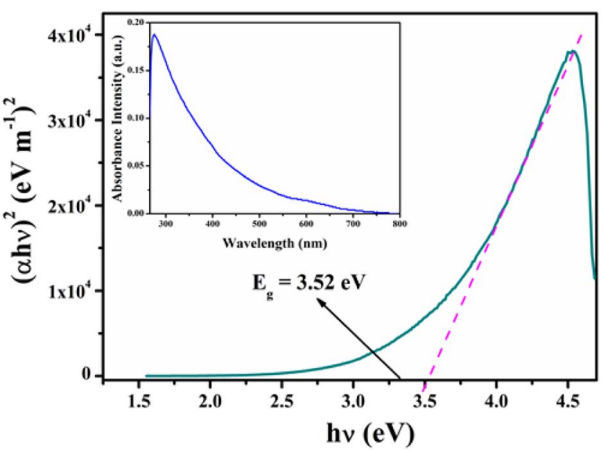

Fig. 8 Optical direct band gap (E_g) and UV-Vis absorption spectra (inset) of the metallogel.

Fig. 9 shows the *I–V* graph of our fabricated MBDs from where the conductivity (σ) was computed as 7.38×10^{-5} S m^{-1}, which signifies our Zn-AA metallogel as a typical semiconductor. The *I–V* graph of MBD (Fig. 9) represents nonlinear rectifying behavior which depicts the development of the Schottky barrier diode at the Al/metallogel boundary. So, in this article, we showed our attention to studying the properties of transporting charge of MBD and further discussed them elaborately. The on/off (rectification) ratio of our device (I_{on}/I_{off}) at ±2 V was calculated from the *I–V* graph (Fig. 9) as 49.63. The obtained *I–V* graph of MBD was analyzed in detail utilizing thermionic emission theory. Hence, Cheung's method was implemented to compute some important parameters of diode.[60–63]

By using thermionic emission theory, we were able to get a deeper understanding of the *I–V* characteristic of metallogel based device (MBD). Important diode parameters were also extracted using Cheung's method.[60] Accordingly, we performed a quantitative analysis of the acquired *I–V* curve using the following reference eqn (2) and (3):[61,62]

$$I = I_0 \exp\left(\frac{qV}{\eta kT}\right)\left[1 - \exp\left(\frac{-qV}{\eta kT}\right)\right] \quad (2)$$

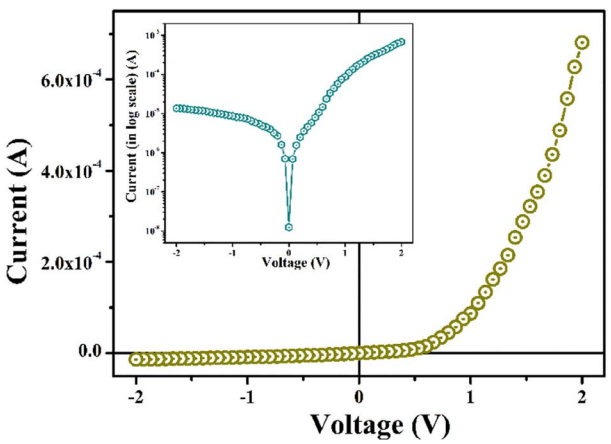

Fig. 9 *I–V* characteristics graph of MBD.

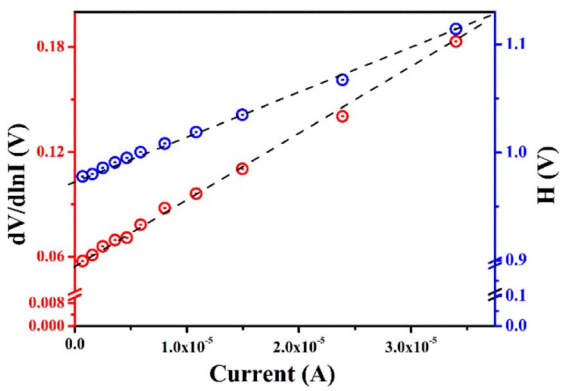

Fig. 10 d*V*/d ln *I* *vs.* *I* and *H* *vs.* *I* graph of MBD.

Table 1 Various parameters of Schottky device (Zn-AA based)

Device	On/off	Conductivity (S m^{-1})	Ideality factor (η)	Barrier height ($\varnothing_B$) (eV)	Series resistance (R_S) From dV/d ln I *vs.* I (KΩ)	Series resistance (R_S) From H *vs.* I (KΩ)
Zn-AA metallogel based device	49.63	7.38×10^{-5}	2.16	0.45	3.79	4.01

$$I_0 = AA^*T^2 \exp\left(\frac{-q\varnothing_B}{kT}\right) \quad (3)$$

where, I_0 stands for saturation current, A^* is effective Richardson constant, η is ideality factor, A denotes effective diode area, V represents forward bias voltage, T is the absolute temperature in Kelvin, q is the electronic charge and k is the Boltzmann constant. The functional Richardson constant was taken into account for all the devices as 32 A K^{-2} cm^{-2} and the active diode area was determined to be 7.065×10^{-2} cm^2.[60]

Eqn (4)–(6), derived from Cheung's concept, were also used to calculate the series resistance (R_S), ideality factor (η) and potential barrier height ($\varnothing_B$).[62,63]

$$\frac{dV}{d\ln(I)} = \left(\frac{\eta kT}{q}\right) + IR_S \quad (4)$$

$$H(I) = V - \left(\frac{\eta kT}{q}\right)\ln\left(\frac{I_S}{AA^*T^2}\right) \quad (5)$$

$$H(I) = IR_S + \eta\varnothing_B \quad (6)$$

The ideality factor (η) for MBD was calculated as 2.16, from the intercept of the dV/d ln I *vs.* I graph (Fig. 10). From the slope of the same plotting, the series resistance (R_S) of MBD was also calculated as 3.79 KΩ. A fluctuation from the ideal value (~1) for the computed η is shown for MBD. This deviation symbolizes the barrier height inhomogeneities with the presence of juncture states and series resistance at the MS junction.[64,65]

The barrier height ($\varnothing_B$) of MBD was estimated as 0.45 eV from the intercept of H *vs.* current graph (Fig. 10) and utilizing the just computed η [eqn (6)]. The R_S of MBD was also computed from the slope of this graph and it was calculated as 4.01 KΩ. Table 1 presents all the values of the computed parameters of MBD. The obtained values of R_S from the different two graphs are very near about.

For an in-depth explanation of the moving of the charge carriers at the MS boundary, we plotted the I–V curves on a logarithmic scale. In the ln(I) *vs.* ln(V) graph of MBD, two distinctive slopes are seen (Fig. 11). These two distinctive slope regions were represented as region-I and region-II. In region-I, the value of the slope is ~1, indicating the ohmic regime. In this region, the generated current follows the $I \propto V$ relation. On the other hand, the value of slope in region-II is ≥ 2 and the generated current follows the $I \propto V^2$ relation (Fig. 11). Hence region-II is contemplated as a space charge limited current (SCLC) region that is devoid of trap.[60,66] If the inherent charge transporters are less than the inserted charge transporters, a space charge field is produced due to the expanding of the inserted charge transporters. This generated charge field governs the produced currents so it is called space charge limited current or SCLC.[60,66] To estimate the performance of MBD, in this article we employed this theory. Hence to compute the effective carrier mobility from region-II, the equation of Mott–Gurney was considered and I *vs.* V^2 graph (Fig. 12) has been drawn:[60,63,66]

$$I = \frac{9\mu_{eff}\varepsilon_0\varepsilon_r A}{8}\left(\frac{V^2}{d^3}\right) \quad (7)$$

where, ε_0, ε_r, μ_{eff} and I symbolize their usual meaning. The relative dielectric constants value of the metallogel was considered as 2.25.[67]

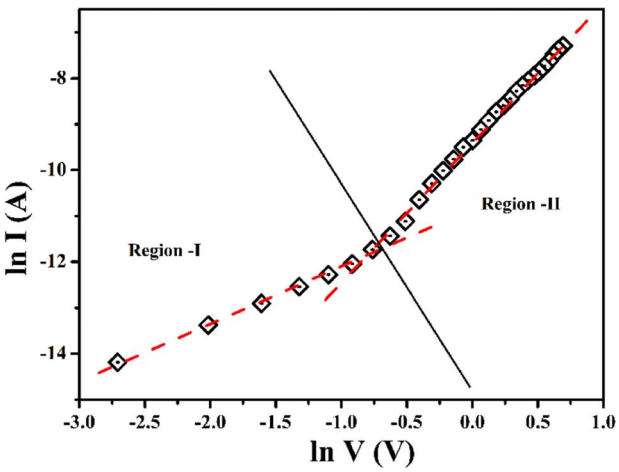

Fig. 11 ln I *vs.* ln V graph of MBD.

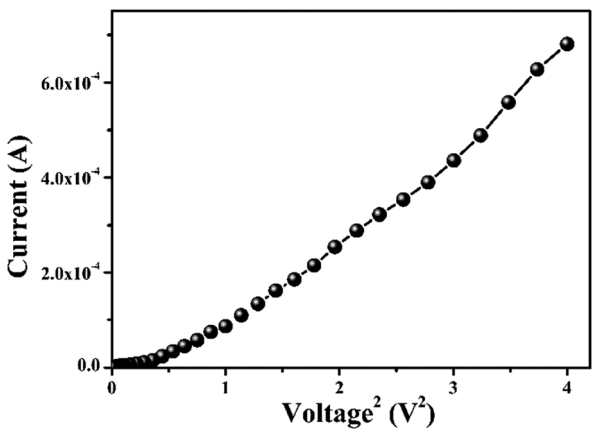

Fig. 12 I *vs.* V^2 graph of MBD.

Table 2 Various charge conducting parameters of MBD

Device	ε_r	μ_{eff} ($m^2\ V^{-1}\ s^{-1}$)	τ (sec)	$\mu_{eff}\tau$ ($m^2\ V^{-1}$)	D ($m^2\ s^{-1}$)	L_D (m)
Zn-AA metallogel based device	2.25	1.08×10^{-6}	3.21×10^{-9}	3.46×10^{-13}	2.78×10^{-8}	1.34×10^{-7}

Table 3 Comparison table of electrical parameters of Zn-AA metallogel based device with other reported results

Device based on	On/off	Ideality factor	Barrier height (eV)	Series resistance (KΩ)	Ref.
$[Zn(INH)(succ)]_n$	176	1.43	0.36	—	68
ZnCdS	29	2.22	—	17.3	69
$[Cd(4bpd)(SCN)_2]_n$	46.55	5.52	0.36	—	70
$C_{40}H_{34}Cu_2N_6O_{18}$	8.46	2.78	0.47	—	71
$[Cd_4L_2(NCO)_6]_n$	12.44	3.47	0.526	5.31	72
Zn-AA metallogel	49.63	2.16	0.45	3.79	Present work

The diffusion length (L_D) and transit time (τ) were also computed to study the transportation phenomenon of the charge carrier across the junction. The transit time (τ) value has been computed from eqn (8).[60]

$$\tau = \frac{9\varepsilon_0\varepsilon_r A}{8d}\left(\frac{V}{I}\right) \quad (8)$$

$$\mu_{eff} = \frac{qD}{kT} \quad (9)$$

$$L_D = \sqrt{2D\tau} \quad (10)$$

Here, D represents the diffusion coefficient and was computed using the Einstein–Smoluchowski equation (eqn (9)).[60] L_D of charge carriers acts a crucial role in device performance when an MS junction is developed and was computed from the eqn (10). All the calculated parameters are shown in Table 2.

We have compared the parameters of our fabricated semiconductor device with other reported various semiconductor devices and presented in Table 3.

From the Table 3 it is clear that the ideal factor of our fabricated semiconductor device is more ideal (~1) than the other reported semiconductor devices. Moreover, the barrier height of our device is less than 0.5 eV, which means this device can work under very small applied voltage. Even, the series resistance is lower for this device compared to other devices. This proves that the performance of our fabricated device is better than the other devices.

4. Conclusions

In conclusion, rapid mixing of zinc acetate and a low molecular weight gelator adipic acid in DMF solvent medium followed by sonication yielded a new supramolecular Zn(II)-metallogel at room temperature. Zn-AA metallogel is created by a variety of non-covalent interactions that allow it to be stable at ambient conditions. Zn-AA metallogel's hierarchical structure, which resembles flakes, was investigated using the field emission scanning electron microscopy (FESEM) as well as the transmission electron microscopy (TEM) instruments. The rheological tests have analysed the mechanical strength of the Zn-AA metallogel. The measurements of optical band gap of our generated Zn-AA metallogel are consistent with a semiconducting state. Also, we used semiconducting Zn-AA metallogel and Au metal to create a metal–semiconductor junction thin film device. Fabrication of a Schottky diode was verified by the current–voltage (I–V) characteristic graph, which demonstrated the device's nonlinear charge transport. Therefore, the current investigation of a sandwich-like configuration of the indium tin oxide (ITO), zinc acetate-adipic acid (Zn-AA) metallogel, and gold (Au) hints to the potential for developing supramolecular Zn^{2+} metallogel-based electrical devices for cutting-edge technology in the future. In actuality, the adipic acid and zinc(II) source based Zn-AA metallogel study is a pioneering strategy and symbolise metallogel for the fabrication of the semiconducting device.

Conflicts of interest

The authors declare no competing financial interests.

Acknowledgements

K. K. is grateful to the University Grant Commission, New Delhi, for awarding him Junior Research Fellowship (Award letter number: 63/(CSIR-UGC NET June 2019)). S. D. is thankful to the UGC, New Delhi, for awarding him Dr D. S. Kothari Postdoctoral Fellowship (Award letter number: No. F.4-2/2006 (BSR)/CH/19-20/0224). S. B. thankfully acknowledges DST Inspire Faculty Research Grant (Faculty Registration No.: IFA18-CH304; DST/INSPIRE/04/2018/000329).

Notes and references

1 N. M. Sangeetha and U. Maitra, *Chem. Soc. Rev.*, 2005, **34**, 821–836.
2 P. Dastidar, *Chem. Soc. Rev.*, 2008, **37**, 2699–2715.
3 M. D. Ward, *Chem. Soc. Rev.*, 1997, **26**, 365–375.

4 R. Madueno, M. T. Räisänen, C. Silien and M. Buck, *Nature*, 2008, **454**, 618–621.
5 P. Terech and R. G. Weiss, *Chem. Rev.*, 1997, **97**, 3133–3159.
6 S. Dhibar, A. Dey, A. Dey, S. Majumdar, A. Mandal, P. P. Ray and B. Dey, *New J. Chem.*, 2019, **43**, 15691–15699.
7 C. K. Karan and M. Bhattacharjee, *ACS Appl. Mater. Interfaces*, 2016, **8**, 5526–5535.
8 Q. Lin, Q. P. Yang, B. Sun, Y. P. Fu, X. Zhu, T. B. Weia and Y. M. Zhang, *Soft Matter*, 2014, **10**, 8427–8432.
9 X. Ma, S. Liu, Z. Zhang, Y. Niu and J. Wu, *Soft Matter*, 2017, **13**, 8882–8885.
10 C. Po, Z. Ke, A. Y. Y. Tam, H. F. Chow and V. W. W. Yam, *Chem.–Eur. J.*, 2013, **19**, 15735–15744.
11 S. Dhibar, A. Dey, D. Ghosh, S. Majumdar, A. Dey, P. Mukherjee, A. Mandal, P. P. Ray and B. Dey, *ChemistrySelect*, 2019, **4**, 1535–1541.
12 R. M. Ortuño, *Gels*, 2021, **7**, 54.
13 C. A. Offiler, C. D. Jones and J. W. Steed, *Chem. Commun.*, 2017, **53**, 2024–2027.
14 B. Jiang, J. Zhang, W. Zheng, L. J. Chen, G. Q. Yin, Y. X. Wang, B. Sun, X. Li and H. B. Yang, *Chem.–Eur. J.*, 2016, **22**, 14664–14671.
15 H. Bunzen, Nonappa, E. Kalenius, S. Hietala and E. Kolehmainen, *Chem.–Eur. J.*, 2013, **19**, 12978–12981.
16 K. Mitsumoto, J. M. Cameron, R. J. Wei, H. Nishikawa, T. Shiga, M. Nihei, G. N. Newton and H. Oshio, *Chem.–Eur. J.*, 2017, **23**, 1502–1506.
17 F. Gou, J. Cheng, X. Zhang, G. Shen, X. Zhou and H. Xiang, *Eur. J. Inorg. Chem.*, 2016, **2016**, 4862–4866.
18 X. Q. Wang, W. Wang, G. Q. Yin, Y. X. Wang, C. W. Zhang, J. M. Shi, Y. Yu and H. B. Yang, *Chem. Commun.*, 2015, **51**, 16813–16816.
19 S. J. Wezenberg, C. M. Croisetu, M. C. A. Stuart and B. L. Feringa, *Chem. Sci.*, 2016, **7**, 4341–4346.
20 R. Luboradzki and Z. Pakulski, *Tetrahedron*, 2004, **60**, 4613–4616.
21 J. H. Jung, G. John, M. Masuda, K. Yoshida, S. Shinkai and T. Shimizu, *Langmuir*, 2001, **17**, 7229–7232.
22 M. George, G. Tan, V. T. John and R. G. Weiss, *Chem.–Eur. J.*, 2005, **11**, 3243–3254.
23 S. Samai, J. Dey and K. Biradha, *Soft Matter*, 2011, **7**, 2121–2126.
24 C. Tomasini and N. Castellucci, *Chem. Soc. Rev.*, 2013, **42**, 156–172.
25 P. Babu, N. M. Sangeetha and U. Maitra, *Macromol. Symp.*, 2006, **241**, 60–67.
26 C. Narayana, R. K. Upadhyay, R. Chaturvedia and R. Sagar, *New J. Chem.*, 2017, **41**, 2261–2267.
27 J. Yan, J. Liu, P. Jing, C. Xu, J. Wu, D. Gao and Y. Fang, *Soft Matter*, 2012, **8**, 11697–11703.
28 C. C. Tsou and S. S. Sun, *Org. Lett.*, 2006, **8**, 387–390.
29 Q. Lin, T. T. Lu, X. Zhu, B. Sun, Q. P. Yang, T. B. Weia and Y. M. Zhang, *Chem. Commun.*, 2015, **51**, 1635–1638.
30 X. Ji, Y. Yao, J. Li, X. Yan and F. Huang, *J. Am. Chem. Soc.*, 2013, **135**, 74–77.
31 S. M. Mehta, T. Jin, I. Stanciulescu and K. J. Grande-Allen, *Acta Biomater.*, 2018, **75**, 52–62.
32 B. Escuder, F. Rodríguez-Llansola and J. F. Miravet, *New J. Chem.*, 2010, **34**, 1044–1054.
33 X. Cheng, J. Pan, Y. Zhao, M. Liao and H. Peng, *Adv. Energy Mater.*, 2018, **8**, 1702184–1702199.
34 X.-Q. Dou and C.-L. Feng, *Adv. Mater.*, 2017, **29**, 1604062–1604082.
35 N. Shi, G. Yin, M. Han and Z. Xu, *Colloids Surf., B*, 2008, **66**, 84–89.
36 A. R. Hirst, B. Escuder, J. F. Miravet and D. K. Smith, *Angew. Chem., Int. Ed.*, 2008, **47**, 8002–8018.
37 J. Wang, Z. Wang, J. Gao, L. Wang, Z. Yang, D. Kong and Z. Yang, *J. Mater. Chem.*, 2009, **19**, 7892–7896.
38 J. Boekhoven and S. I. Stupp, *Adv. Mater.*, 2014, **26**, 1642–1659.
39 X. Jiaa and K. L. Kiick, *Macromol. Biosci.*, 2009, **9**, 140–156.
40 P. R. A. Chivers and D. K. Smith, *Nat. Rev. Mater.*, 2019, **4**, 463–478.
41 O. Roubeau, A. Colin, V. Schmitt and R. Clérac, *Angew. Chem., Int. Ed.*, 2004, **43**, 3283–3286.
42 V. K. Pandey, M. K. Dixit, S. Manneville, C. Bucherc and M. Dubey, *J. Mater. Chem. A*, 2017, **5**, 6211–6218.
43 Y.-X. Ye, W.-L. Liu and B.-H. Ye, *Catal. Commun.*, 2017, **89**, 100–105.
44 W. Miao, L. Zhang, X. Wang, H. Cao, Q. Jin and M. Liu, *Chem.–Eur. J.*, 2013, **19**, 3029–3036.
45 S. Dhibar, A. Dey, S. Majumdar, D. Ghosh, A. Mandal, P. P. Ray and B. Dey, *Dalton Trans.*, 2018, **47**, 17412–17420.
46 J. Gómez-Herrero and F. Zamora, *Adv. Mater.*, 2011, **23**, 5311–5317.
47 H. Su, S. Zhu, M. Qu, R. Liu, G. Song and H. Zhu, *J. Phys. Chem. C*, 2019, **123**, 15685–15692.
48 P. Sutar and T. K. Maji, *Chem. Commun.*, 2016, **52**, 8055–8074.
49 S. Dhibar, A. Dey, S. Majumdar, A. Dey, P. P. Ray and B. Dey, *Ind. Eng. Chem. Res.*, 2020, **59**, 5466–5473.
50 S. Dhibar, A. Dey, A. Dey, S. Majumdar, D. Ghosh, P. P. Ray and B. Dey, *ACS Appl. Electron. Mater.*, 2019, **19**, 1899–1908.
51 S. Dhibar, R. Jana, P. P. Ray and B. Dey, *J. Mol. Liq.*, 2019, **289**, 111126.
52 N. Malviya, C. Sonkar, R. Ganguly and S. Mukhopadhyay, *Inorg. Chem.*, 2019, **58**, 7324–7334.
53 S. Dey, D. Datta, K. Chakraborty, S. Nandi, A. Anoop and T. Pathak, *RSC Adv.*, 2013, **3**, 9163–9166.
54 S. Saha, E.-M. Schön, C. Cativiela, D. D. Díaz and R. Banerjee, *Chem.–Eur. J.*, 2013, **19**, 9562–9568.
55 S. Dhibar, S. K. Ojha, A. Mohan, S. P. C. Prabhakaran, S. Bhattacharjee, K. Karmakar, P. Karmakar, P. Predeep, A. K. Ojha and B. Saha, *New J. Chem.*, 2022, **46**, 17189–17200.
56 S. Enthaler, *ACS Catal.*, 2013, **3**, 150–158.
57 A. Biswas, S. Mukhopadhyay, R. S. Singh, A. Kumar, N. K. Rana, B. Koch and D. S. Pandey, *ACS Omega*, 2018, **3**, 5417–5425.
58 R. Leuci, L. Brunetti, A. Laghezza, F. Loiodice, P. Tortorella and L. Piemontese, *Appl. Sci.*, 2020, **10**, 4118.
59 H. Wu, J. Zheng, A. L. Kjøniksen, W. Wang, Y. Zhang and J. Ma, *Adv. Mater.*, 2019, **31**, 1806204.

60 A. Dey, S. Middya, R. Jana, M. Das, J. Datta, A. Layek and P. P. Ray, *J. Mater. Sci.: Mater. Electron.*, 2016, **27**, 6325–6335.
61 E. H. Rhoderick, *Metal Semiconductors Contacts*, Oxford University Press, Oxford, 1978.
62 S. K. Cheung and N. W. Cheung, *Appl. Phys. Lett.*, 1986, **49**, 85–87.
63 A. Dey, A. Layek, A. Roychowdhury, M. Das, J. Datta, S. Middya, D. Das and P. P. Ray, *RSC Adv.*, 2015, **5**, 36560–36567.
64 R. K. Gupta and F. Yakuphanoglu, *Sol. Energy*, 2012, **86**, 1539–1545.
65 X. Miao, S. Tongay, M. K. Petterson, K. Berke, A. G. Rinzler, B. R. Appleton and A. F. Hebard, *Nano Lett.*, 2012, **12**, 2745–2750.
66 P. W. M. Blom, M. J. M. de Jong and M. G. van Munster, *Phys. Rev. B: Condens. Matter Mater. Phys.*, 1997, **55**, R656–R659.
67 S. Dhibar, A. Dey, S. Majumdar, P. P. Ray and B. Dey, *Int. J. Energy Res.*, 2020, **45**, 5486–5499.
68 K. Naskar, A. Dey, B. Dutta, F. Ahmed, C. Sen, M. H. Mir, P. P. Ray and C. Sinha, *Cryst. Growth Des.*, 2017, **17**, 3267–3276.
69 M. Das, J. Datta, R. Jana, S. Sil, S. Halder and P. P. Ray, *New J. Chem.*, 2017, **41**, 5476–5486.
70 S. Halder, A. Dey, A. Bhattacharjee, J. Ortega-Castro, A. Frontera, P. P. Ray and P. Roy, *Dalton Trans.*, 2017, **46**, 11239–11249.
71 A. Hossain, A. Dey, S. K. Seth, P. P. Ray, P. Ballester, R. G. Pritchard, J. Ortega-Castro, A. Frontera and S. Mukhopadhyay, *ACS Omega*, 2018, **3**, 9160–9171.
72 P. Ghorai, A. Dey, P. Brandão, J. Ortega-Castro, A. Bauza, A. Frontera, P. P. Ray and A. Saha, *Dalton Trans.*, 2017, **46**, 13531–13543.